Appl. Math. Mech. -Engl. Ed., **42**(7), 915–930 (2021)

APPLIED MATHEMATICS AND MECHANICS (ENGLISH EDITION)

https://doi.org/10.1007/s10483-021-2744-7

The size-dependent elastohydrodynamic lubrication contact of a coated half-plane with non-Newtonian fluid*

Jie SU[1], Hongxia SONG[2], Liaoliang KE[1,†], S. M. AIZIKOVICH[3]

1. School of Mechanical Engineering, Tianjin University, Tianjin 300350, China;
2. School of Mathematical Science, Inner Mongolia University, Hohhot 010021, China;
3. Laboratory of Functionally Graded and Composite Materials, Research and Education Center "Materials", Don State Technical University, Rostov-on-Don 344000, Russia

(Received Jan. 30, 2021 / Revised Apr. 6, 2021)

Abstract Based on the couple-stress theory, the elastohydrodynamic lubrication (EHL) contact is analyzed with a consideration of the size effect. The lubricant between the contact surface of a homogeneous coated half-plane and a rigid punch is supposed to be the non-Newtonian fluid. The density and viscosity of the lubricant are dependent on fluid pressure. Distributions of film thickness, in-plane stress, and fluid pressure are calculated by solving the nonlinear fluid-solid coupled equations with an iterative method. The effects of the punch radius, size parameter, coating thickness, slide/roll ratio, entraining velocity, resultant normal load, and stiffness ratio on lubricant film thickness, in-plane stress, and fluid pressure are investigated. The results demonstrate that fluid pressure and film thickness are obviously dependent on the size parameter, stiffness ratio, and coating thickness.

Key words elastohydrodynamic lubrication (EHL), non-Newtonian fluid, size effect, couple-stress theory, coating

Chinese Library Classification O373
2010 Mathematics Subject Classification 76A05

1 Introduction

Coatings on the contact surface can reduce mismatching stresses, resist contact damage, improve the wear resistance and corrosion resistance, and possess thermal shielding functions. Therefore, coatings are commonly applied in various devices, such as turbines, transducers, actuators, bearings, gears, furnace liners, sensors, micro-electronics, and micro-power generators[1–2]. In addition, coatings can also be used to improve surface performance of elastohydrodynamic lubrication (EHL) contact. In general, lubricants and coatings are

* Citation: SU, J., SONG, H. X., KE, L. L., and AIZIKOVICH, S. M. The size-dependent elastohydrodynamic lubrication contact of a coated half-plane with non-Newtonian fluid. *Applied Mathematics and Mechanics* (*English Edition*), **42**(7), 915–930 (2021) https://doi.org/10.1007/s10483-021-2744-7

† Corresponding author, E-mail: llke@tju.edu.cn

Project supported by the National Natural Science Foundation of China (Nos. 11902217, 11725207, and 12011530056) and the Russian Foundation for Basic Research (No. 20-58-53045-GFEN-a)

employed together to improve contact damage and wear of the material surface. Hence, the dry contact and EHL contact of coatings have attracted much attention[3–4]. The dry contact of coatings can be found in the frictionless contact[5], sliding frictional contact[6], receding contact[7], adhesive contact[8], and fretting contact[9]. The EHL contact and thermal EHL contact were numerically investigated for the homogeneous elastic coating[4,10–11].

However, when the coating thickness or contact scale is reduced from macro-scales to micro-/nano-scales, the contact behaviors of coating may be influenced by the size effect. The size effect of micro-/nano-structures is important for contact behaviors and cannot be ignored[12]. Unfortunately, the classical elasticity theory is not efficient to evaluate the size effect of materials at micro-/nano-scales. To involve the characteristic material length in constitutive relations, the couple-stress elasticity theory is employed to examine the size-dependent contact[13–14]. In addition to normal and tangential forces, couple stresses, i.e., moments per unit area, act on the volume element surfaces. Curvature (i.e., gradient of the rotation) and characteristic material length are introduced to describe the additional deformation and micro-structure of materials in the couple stress elasticity theory[15–16].

Regarding to homogeneous isotropic elastic half-plane, Zisis et al.[14] first analyzed the frictionless contact by applying the couple-stress elasticity theory. They found that contact behaviors at micro-/nano-scales were significantly influenced by the characteristic material length. Similar contact for the homogeneous elastic half-plane was later investigated for some typical punches[17]. By combining the generalized stress function method with the couple-stress elasticity theory, the steady-state thermo-mechanical contact was investigated with a consideration of the heat flux[18]. The sliding frictional contact and partial slip contact were examined with the couple-stress elasticity theory[19–20]. By using nano-indentation and scratch tests, the macro-/nano-mechanical behaviors of coatings were analyzed by Bhattacharyya and Mishra[21]. The size-dependent indentation was discussed by Karuriya and Bhandakkar[22] for an elastic layer under three kinds of rigid punches. Song et al.[23] studied two-dimensional frictionless contact for the coating according to the couple-stress elasticity theory.

So far, the investigations are mostly about the size-dependent dry contact of the coating. The miniaturization of mechanical components in the micro-/nano-engineering field results in the micro-/nano-scale EHL contact existing widely in bearings and gears[24]. Thus, it is essential to accurately describe the EHL contact of coatings at micro-/nano-scales. While, the size-dependent EHL contact is rarely reported. The micro-EHL line contact between two deformable cylinders with coatings was investigated by considering the Eyring-type fluid model[25]. Thermal micro-EHL of a crowned gear pair was investigated under heavy-load and high-speed operating conditions[26]. Influences of rough surface, non-Newtonian and transient temperature on lubricant thickness, pressure, temperature rise, and friction coefficient were discussed in-depth. Shirvani et al.[27] studied the EHL contact with surface roughness to improve friction and lubrication performance at nano-scale. For the EHL line contact problem, Woloszynski et al.[28] discussed the influence of nano-scale roughness by using ball-on-disc experiments and numerical simulations. Checo et al.[29] introduced a homogenized micro-EHL contact model which took into account the micro-scale deformation and non-negligible pressure. However, the EHL contact mentioned above did not take the size effect into account.

In fact, an effective EHL model should include the non-Newtonian fluid behavior caused by high shear rates[30]. The shear thinning or viscosity loss effects of non-Newtonian fluid have been described by a variety of rheological models[31], such as the nonlinear viscous model (Ree-Eyring model)[32], the nonlinear visco-elastic model (J-T model)[33], and the nonlinear visco-plastic model[34]. Since the Ree-Eyring model is relatively simple, this model has been adopted widely in numerical analysis of EHL problems[35–36].

Previous investigations are mostly focused on the size-dependent dry contact or macro-scale EHL contact of coatings. Based on the couple-stress elasticity theory, we further study the

size-dependent EHL line contact of a homogeneous coated half-plane. The viscosity and density of non-Newtonian fluid lubricant are dependent on the fluid pressure. The generalized stress function method is used to calculate the normal displacement on the surface for size-dependent dry contact of a coated half-plane. Subsequently, an iterative method is used to handle flow rheology equation, film thickness equation, load balance equation, and Reynolds equation. Influences of punch radius, size parameter, coating thickness, slide/roll ratio, entraining velocity, resultant normal load, and stiffness ratio on EHL contact behaviors are illustrated.

This paper makes the first attempt to analyze the size effect on the EHL line contact between a coated half-plane and a rigid cylindrical punch. We highlight new aspects as follows. (i) A size-dependent EHL contact model is first developed in this paper. This model can be used to evaluate the effect of size parameter on the fluid pressure, in-plane stress, and film thickness. (ii) The effect of non-Newtonian fluid is considered in size-dependent EHL contact for the first time. By using the Ree-Eyring model, the viscosity loss effect of non-Newtonian fluid can be described. The influence of slide/roll ratio on fluid pressure, frictional coefficient, and shear stress at coating surface is illustrated.

2 Theoretical formulations

Figure 1 illustrates a homogeneous elastic coated half-plane for the size-dependent EHL line contact. The lubricant is supposed to be the non-Newtonian fluid. P and R are the normal load and punch radius. The homogeneous elastic half-plane is perfectly bonded to the coating with the thickness H. Sliding velocities are V_1 and V_2 for punch and half-plane, respectively.

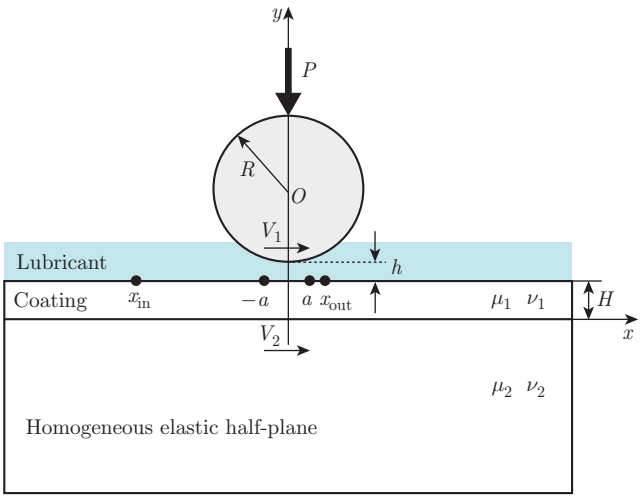

Fig. 1 Sketch of size-dependent EHL line contact between rigid cylindrical punch and homogeneous coated half-plane based on couple-stress elasticity theory (color online)

2.1 Couple-stress elasticity theory

The geometric equations between strain components (ε_{xxi}, ε_{yyi}, ε_{xyi}, and ε_{yxi}) and displacement components (u_{xi} and u_{yi}) can be found in Eq. (2) of Ref. [23] within the two-dimensional linearized couple-stress elasticity theory in the plane stain state. The geometric equations for the homogeneous half-plane and coating about the rotation $\omega_i = \omega_{zi}$ are expressed as

$$k_{xzi} = \frac{\partial \omega_i}{\partial x}, \quad k_{yzi} = \frac{\partial \omega_i}{\partial y}, \quad \omega_i = \frac{1}{2}\Big(\frac{\partial u_{yi}}{\partial x} - \frac{\partial u_{xi}}{\partial y}\Big), \tag{1}$$

where superscripts $i = 1, 2$ represent the coating ($0 < y \leqslant H$) and half-plane ($y \leqslant 0$), respectively; k_{xzi} and k_{yzi} are the curvature tensor components.

The relationships between stress components (σ_{xxi}, σ_{yyi}, σ_{xyi}, and σ_{yxi}) and strain components (ε_{xxi}, ε_{yyi}, ε_{xyi}, and ε_{yxi}) can be found in Eqs. (6)–(8) of Ref. [23], and the relationships of couple stress components (m_{xzi} and m_{yzi}) and curvature tensor components (k_{xzi} and k_{yzi}) can be written as[14,37]

$$k_{xzi} = m_{xzi}/(4\mu_i l_i^2), \tag{2}$$

$$k_{yzi} = m_{yzi}/(4\mu_i l_i^2), \tag{3}$$

where l_i, ν_i, and μ_i are the characteristic material length, Poisson's ratio, and shear modulus, respectively.

The equilibrium equations can be given in Eqs. (3)–(5) of Ref. [23]. It is noticed that the stresses σ_{xyi} and σ_{yxi} are asymmetric in the couple-stress elasticity theory.

2.2 Reynolds equation, load balance equation, and rheology equation

A Ree-Eyring fluid with the nonlinear viscous model is used as the lubricant between two solids. The rheological law of the Ree-Eyring fluid is described as[32,36]

$$\frac{\partial V}{\partial y} = f(\tau, \eta) = \frac{\tau_0}{\eta} \sinh\Big(\frac{\tau}{\tau_0}\Big), \tag{4}$$

where V is the velocity component along the x-direction; $\frac{\partial V}{\partial y}$ is the velocity gradient (i.e., shear strain rate); $\tau = \tau_x$ is the shear stress component; η is the fluid viscosity. The Eyring stress τ_0 is irrelevant to the temperature and fluid pressure, and indicates the transformation from Newtonian fluid to the non-Newtonian fluid. When τ_0 is infinite, the Ree-Eyring fluid is changed to the Newtonian fluid.

The Reynolds equation was modified to describe the non-Newtonian fluid by Yang and Wen[38]. The generalized Reynolds equation of the EHL line contact is obtained, i.e.,

$$\frac{\mathrm{d}}{\mathrm{d}x}\Big(\Big(\frac{\rho}{\eta}\Big)_e h^3 \frac{\mathrm{d}p}{\mathrm{d}x}\Big) = 12 V_0 \frac{\mathrm{d}(\rho^* h)}{\mathrm{d}x}, \tag{5a}$$

where $V_0 = (V_1 + V_2)/2$, p, ρ, and h are the entraining velocity, fluid pressure, fluid density, and film thickness, respectively. We have the following relations:

$$\begin{cases} (\rho/\eta)_e = 12\left(-\rho_e'' + \eta_e \rho_e'/\eta_e'\right), \quad \rho^* = \left(-\rho_e' \eta_e V_0 S + \rho_e V_2\right)/V_0, \quad \rho_e = \displaystyle\int_0^h \rho(x)\mathrm{d}y/h, \\ \rho_e' = \dfrac{1}{h^2}\displaystyle\int_0^h \rho(x) \int_0^y \frac{\mathrm{d}y'}{\eta^*(x,y')}\mathrm{d}y, \quad \rho_e'' = \dfrac{1}{h^3}\displaystyle\int_0^h \rho(x) \int_0^y \frac{y'\mathrm{d}y'}{\eta^*(x,y')}\mathrm{d}y, \\ \eta_e = h \Big/ \displaystyle\int_0^h \frac{\mathrm{d}y}{\eta^*(x,y)}, \quad \eta_e' = h^2 \Big/ \displaystyle\int_0^h \frac{y\mathrm{d}y}{\eta^*(x,y)}, \end{cases} \tag{5b}$$

where $S = 2(V_2 - V_1)/(V_1 + V_2)$ is the slide-roll ratio, changing from 0 (pure rolling conditions) to 2 (pure sliding conditions). For the Newtonian fluid, i.e., $\eta^* = \eta$, Eq. (6) is reduced to the one given by Dowson[39]. For the Ree-Eyring fluid, Yang and Wen obtained the equivalent viscosity η^*[38],

$$\eta^*(x, y) = \frac{\tau}{f(\tau, \eta)} = \frac{\eta\tau/\tau_0}{\sinh(\tau/\tau_0)}, \tag{6}$$

where τ_1 is the shear stress at coating surface,

$$\tau = \tau_1 + y\frac{\mathrm{d}p}{\mathrm{d}x}, \quad \tau_1 = \tau_0 \ln \frac{\sqrt{(V_2 - V_1)^2 + (F_1^2 - F_2^2)} - (V_2 - V_1)}{F_1 + F_2}, \quad V_2 \geqslant V_1,$$

$$F_1 = \int_0^h \frac{\tau_0}{\eta} \cosh\Big(\frac{y}{\tau_0}\frac{\mathrm{d}p}{\mathrm{d}x}\Big)\mathrm{d}y, \quad F_2 = \int_0^h \frac{\tau_0}{\eta} \sinh\Big(\frac{y}{\tau_0}\frac{\mathrm{d}p}{\mathrm{d}x}\Big)\mathrm{d}y.$$

The Dowson-Higginson pressure-fluid density relation and Roelands pressure-viscosity relation (i.e., rheology equation) can be found in Eqs. (12) and (15) of Ref. [40]. In these equations, fluid viscosity η_0 and fluid density ρ_0 are constants at the ambient temperature and pressure; $Z = \alpha/(5.1 \times 10^{-9}(9.67 + \ln \eta_0))$ is the pressure-viscosity index with α being the pressure-viscosity coefficient[40].

Boundary conditions for p are[38]

$$p(x_{\text{out}}) = p(x_{\text{in}}) = \frac{\mathrm{d}p}{\mathrm{d}x}(x_{\text{out}}) = 0, \tag{7}$$

where x_{in} and x_{out} are fluid inlet and outlet of the EHL contact region, respectively. In general, the EHL contact region (x_{in}, x_{out}) includes the dry contact region $(-a, a)$. The fluid inlet x_{in} is generally assumed to be known. $x_{\text{in}} \geqslant 4a$ is chosen to guarantee sufficient oil supply[41]. At this time, x_{in} has little influence[41]. We choose $x_{\text{in}} = -4.759\,8a$ in this work[40]. But the outlet x_{out} should be solved.

For the EHL contact, the load balance equation requires

$$P = \int_{x_{\text{in}}}^{x_{\text{out}}} p(x)\mathrm{d}x. \tag{8}$$

2.3 Film thickness equation

To derive the film thickness equation, we should first obtain displacement $u_{y1}(x, H)$ of the coating[40]. Figure 2 shows the size-dependent dry contact with contact region $-a \leqslant x \leqslant a$.

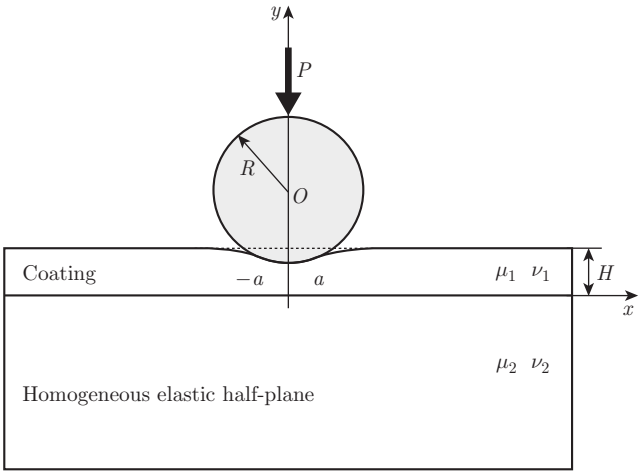

Fig. 2 Sketch of size-dependent dry contact based on couple-stress elasticity theory

Using the generalized stress function method, the surface displacement $u_{y1}(x, H)$ and surface in-plane stress $\sigma_{xx1}(x, H)$ of coated half-plane are obtained in the following integral forms[23]:

$$\begin{aligned} u_{y1}(x, H) = &-\frac{f_{21}}{\pi}\int_{-a}^{a} p^0(t)\int_0^{+\infty} \cos(s(x-t))/s\mathrm{d}s\mathrm{d}t \\ &-\frac{1}{\pi}\int_{-a}^{a} p^0(t)\int_0^{+\infty} (sm_{21}(s, H) - f_{21})\cos(s(x-t))/s\mathrm{d}s\mathrm{d}t, \end{aligned} \tag{9}$$

$$\begin{aligned} \sigma_{xx1}(x, H) = &\frac{1-2\nu_1}{3-2\nu_1}p^0(x) \\ &+\frac{2\mu_1}{\pi(1-\nu_1)}\int_{-a}^{a} p^0(t)\int_0^{\infty} \cos(s(x-t))(\mathrm{i}sm_{11}(s, H) + f_{11})\mathrm{d}s\mathrm{d}t, \end{aligned} \tag{10}$$

where $f_{21}=(1-\nu_1)/(\mu_1(3-2\nu_1))$ and $f_{11}=-1/(\mu_1(6-4\nu_1))$[14,23]; s is the Fourier integral transform variable; $p^0(x)$ is the normal dry contact pressure; the expression of $m_{21}(s,H)$ and $m_{11}(s,H)$ can be found in Eq. (44) of Ref. [23]. For the classical elastic dry contact ($l=0$), we get $f_{21}=(1-\nu_1)/\mu_1$ and $f_{11}=(1-2\nu_1)/(2\mu_1)$[42].

According to the relationship[43]

$$\int_0^\infty s^{-1}\cos(sx)\mathrm{d}s=-\ln|x|, \tag{11}$$

Eq. (9) can be simplified as

$$u_{y1}(x,H)=f_{21}\int_{-a}^{a}\ln|x-t|\,p^0(t)\mathrm{d}t/\pi-\int_{-a}^{a}\Gamma_1(x,t)p^0(t)\mathrm{d}t/\pi, \tag{12}$$

where $\Gamma_1(x,t)=\int_0^{+\infty}(sm_{21}(s,H)-f_{21})\cos(s(x-t))/s\mathrm{d}s$.

For the EHL contact, the fluid pressure is denoted as $p(x)$. By using the parabolic approximation for a cylindrical punch, and according to the surface displacement $u_{y1}(x,H)$ of dry contact in Eq. (12), the lubricant film thickness could be obtained as[40,42]

$$\begin{aligned}h(x)&=\gamma_0+\frac{x^2}{2R}-u_{y1}(x,H)\\&=\gamma_0+\frac{x^2}{2R}-\frac{f_{21}}{2\pi}\int_{x_{\mathrm{in}}}^{x_{\mathrm{out}}}\ln|x-t|^2\,p(t)\mathrm{d}t+\frac{1}{\pi}\int_{x_{\mathrm{in}}}^{x_{\mathrm{out}}}\Gamma_1(x,t)p(t)\mathrm{d}t,\end{aligned} \tag{13}$$

where γ_0 is the rigid displacement at $x=0$.

2.4 Dry contact solution

We use an iterative method to solve Eqs. (5a) and (13) for $p(x)$ and $h(x)$. And $p(x)$ is initially set from the dry contact pressure $p^0(x)$. By using Eq. (12), the governing equation of size-dependent dry contact for a coated half-plane could be given, which yields

$$\frac{\partial u_{y1}(x,H)}{\partial x}=\frac{f_{21}}{\pi}\int_{-a}^{a}\frac{p^0(t)}{x-t}\mathrm{d}t-\frac{1}{\pi}\int_{-a}^{a}p^0(t)\Pi_1(x,t)\mathrm{d}t, \tag{14}$$

where $\Pi_1(x,t)=\frac{\partial\Gamma_1(x,t)}{\partial x}=-\int_0^{+\infty}\sin(s(x-t))(sm_{21}(s,H)-f_{21})\mathrm{d}s$, $|x|\leqslant a$.

For the cylindrical punch, the surface normal displacement in the contact region is approximated as[42]

$$\frac{\partial u_{y1}(x,H)}{\partial x}=\frac{x}{R}. \tag{15}$$

The load balance condition of $p^0(x)$ is

$$\int_{-a}^{a}p^0(t)\mathrm{d}t=P. \tag{16}$$

Using $t=a\theta$, $x=a\tau$, and setting $p^0(\theta)=\lambda(\theta)\sqrt{1-\theta^2}$[44], Eqs. (14) and (16) are described as

$$\sum_{n=1}^{N}(1-\theta_n^2)\left(\frac{f_{21}}{a(\tau_r-\theta_n)}-\Pi_1(\tau_r,\theta_n)\right)\lambda(\theta_n)=\frac{\tau_r}{R}(N+1), \tag{17}$$

$$\sum_{n=1}^{N}(1-\theta_n^2)\lambda(\theta_n)=\frac{(N+1)P}{a\pi}, \tag{18}$$

where $\tau_r=\cos(\pi(2r-1)/(2(N+1)))$, $r=1,2,\cdots,N+1$, and $\theta_n=\cos(\pi n/(N+1))$; N denotes the total number of discrete points.

3 Methodology

3.1 Computing lubricant film thickness

By using uneven mesh discrete nodes $x_{\text{in}} = x_0 < x_1 < \cdots < x_M = x_{\text{out}}$ and Eq. (13), the film thickness is discretized as[40]

$$h_k = \gamma_0 + \frac{x_k^2}{2R} + \delta_k, \tag{19}$$

where

$$\delta_k = \delta(x_k) = \sum_{r=1}^{M-1} (F_{k,r}) p_r, \quad F = \Lambda + Q, \quad k = 0, 1, \cdots, M \tag{20}$$

with M being an even integer. The matrices Q and Λ are determined by computing $-\frac{f_{21}}{2\pi} \int_{x_{\text{in}}}^{x_{\text{out}}} p(t) \ln|x-t|^2 \, \mathrm{d}t$ and $\frac{1}{\pi} \int_{x_{\text{in}}}^{x_{\text{out}}} \Gamma_1(x,t) p(t) \mathrm{d}t$ in Eq. (13), respectively. By applying the interpolation function to approximate fluid pressure[45], δ_k is transformed as

$$\delta_k = \sum_{r=1}^{M-1} (\Lambda_{k,r} + Q_{k,r}) p_r = \sum_{r=1}^{M-1} (\Lambda_{k,r}) p_r + \sum_{r_1=1,3,5}^{M-1} (\overline{Q}_{k,r_1-1} p_{r_1-1} + \overline{Q}_{k,r_1} p_{r_1} + \overline{Q}_{k,r_1+1} p_{r_1+1}), \tag{21}$$

where 'deformation matrix' $\overline{Q}$ can be found in Eq. (79) of Ref. [46] by replacing $f_1/(2\mu)$ with f_{21}.

3.2 Solving Reynolds equation

We could rewrite Eq. (5a) by using the finite difference method[40]

$$\begin{aligned}
&-12V_0 \sum_{n=1}^{M-1} \Big(\Big(\frac{\mathrm{d}\rho^*}{\mathrm{d}x} \Big)_k F_{k,n} + \rho_k^* C_{k,n} \Big) p_n + \Big(\Big(\frac{\mathrm{d}}{\mathrm{d}x} \Big(\Big(\frac{\rho}{\eta} \Big)_e h^3 \Big) \Big)_k A_{k,k-1} + \Big(\frac{\rho}{\eta} \Big)_{ek} h_k^3 B_{k,k-1} \Big) p_{k-1} \\
&+ \Big(\Big(\frac{\mathrm{d}}{\mathrm{d}x} \Big(\Big(\frac{\rho}{\eta} \Big)_e h^3 \Big) \Big)_k A_{k,k} + \Big(\frac{\rho}{\eta} \Big)_{ek} h_k^3 B_{k,k} \Big) p_k \\
&+ \Big(\Big(\frac{\mathrm{d}}{\mathrm{d}x} \Big(\Big(\frac{\rho}{\eta} \Big)_e h^3 \Big) \Big)_k A_{k,k+1} + \Big(\frac{\rho}{\eta} \Big)_{ek} h_k^3 B_{k,k+1} \Big) p_{k+1} \\
&= 12V_0 \Big(\Big(\frac{\mathrm{d}\rho^*}{\mathrm{d}x} \Big)_k \Big(\gamma_0 + \frac{x_k^2}{2R} \Big) + \rho_k^* \frac{x_k}{R} \Big),
\end{aligned} \tag{22}$$

where $C_{k,n}, A_{k,k+1}, A_{k,k}, A_{k,k-1}, B_{k,k+1}, B_{k,k}$, and $B_{k,k-1}$ can be found in Eq. (81) of Ref. [46]. Using Eq. (7), the boundary conditions are $p(x_{\text{in}}) = p_0 = 0$ and $p(x_{\text{out}}) = p_M = 0$.

We use the iterative method to handle coupled equations (6), (8), (19), and (22). The corresponding flow chart is shown in Fig. 3[40].

4 Results and discussion

The chosen material is aluminum for elastic half-plane with $\nu_2 = 0.3$ and $\mu_2 = 27.3\,\text{GPa}$. The pressure-viscosity coefficient, Poisson's ratio of homogeneous coating, fluid film inlet, Eyring stress, pressure under-relaxation factor, fluid viscosity, and revising factor of γ_0 are chosen as $\alpha = 2.19 \times 10^{-8}\,\text{Pa}^{-1}$, $\nu_1 = 0.3$, $x_{\text{in}} = -4.759\,8a$, $\tau_0 = 5\,\text{MPa}$, $\omega_p = 0.15$, $\eta_0 = 0.08\,\text{Pa}\cdot\text{s}$, and $\omega_h = 0.25$[40,47], respectively. Unless otherwise specified, punch radius, stiffness ratio, coating thickness, resultant normal load, size parameter of half-plane, size parameter ratio of coating and half-plane, entraining velocity, and slide/roll ratio are chosen as $R = 100\,\mu\text{m}$, $\mu_1/\mu_2 = 1.2$, $H = 1.0\,\mu\text{m}$, $P = 350\,\text{N/m}$, $l_2 = l = 0.3\,\mu\text{m}$, $l_1/l_2 = 1.0$, $V_0 = 0.5\,\text{mm/s}$, and $S = 0$, respectively. The additional parameter $H_0 = 1.0\,\mu\text{m}$ is introduced for normalization.

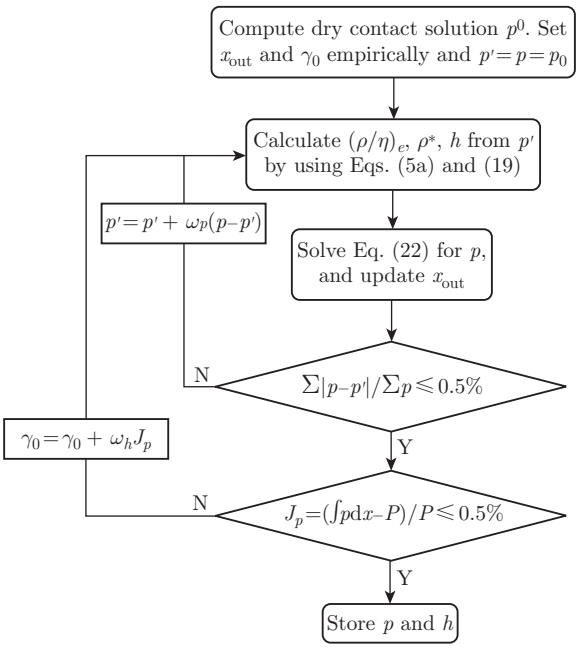

Fig. 3 Flow chart of iterative method

4.1 Comparison and convergence study

By ignoring the lubricant effect, the present EHL contact is reduced to the dry contact with couple stress. Figure 4 shows dry contact pressure $p^0(x)$ for $P = 20\,\mathrm{N/m}$ and $H = 0.1\,\mu\mathrm{m}$, as well as the results by Song et al.[23]. The two results are observed to be in good agreement.

By neglecting the effect of the size parameter, coating, and non-Newtonian fluid, the present EHL contact is reduced to the EHL contact of a homogeneous half-plane in the classical elasticity theory. Figure 5 illustrates the film thickness and fluid pressure with $l = 0$, $H = 0$, $R = 20\,\mathrm{mm}$, $V_0 = 0.6\,\mathrm{m/s}$, $P = 80.8\,\mathrm{kN/m}$, $S = 0$, $\mu_2 = 41\,\mathrm{GPa}$, and $\nu_2 = 0.34$. Meanwhile, the results by Yang and Wen[40] are shown for comparison. Again, both results are found to be in good agreement.

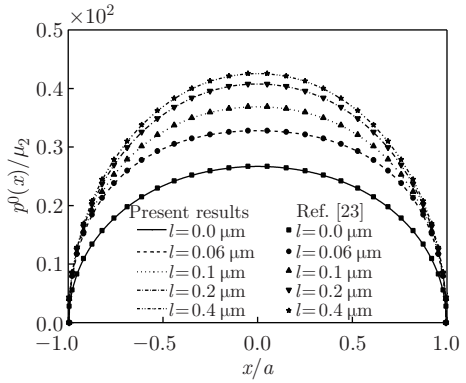

Fig. 4 Comparison of present results and results of Ref. [23]

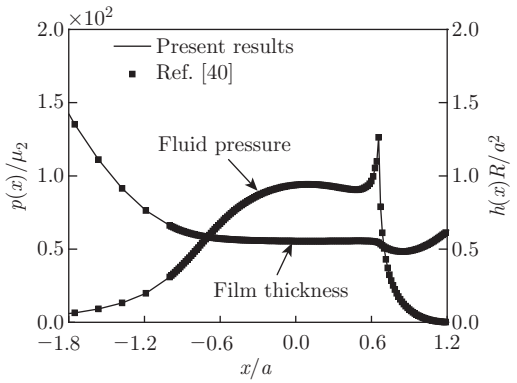

Fig. 5 Comparison of present results and results of Ref. [40]: fluid pressure and film thickness

The influence of the discrete node number M on $h(x)$ and $p(x)$ is analyzed in Fig. 6. With the increase of M, the results of $h(x)$ and $p(x)$ tend to converge. $h(x)$ and $p(x)$ are almost the same for $M = 160$, $M = 180$, and $M = 200$. Thus, the discrete node number is chosen as $M = 180$ in this paper.

Figure 7 illustrates the variation of $h(x)$ and $p(x)$ with different materials. Three different materials, i.e., steel ($\mu_2 = 80.7\,\text{GPa}$ and $\nu_2 = 0.3$), copper ($\mu_2 = 41\,\text{GPa}$ and $\nu_2 = 0.34$), and aluminum ($\mu_2 = 27.3\,\text{GPa}$ and $\nu_2 = 0.3$), are considered in this example. Obviously, the change of material type has a significant effect on fluid pressure at the whole contact region. However, it has slight effect on $h(x)$ at the contact center. The pressure spike is sensitive to shear modulus of materials. It is found that aluminum (steel) has the minimum (maximum) pressure spike.

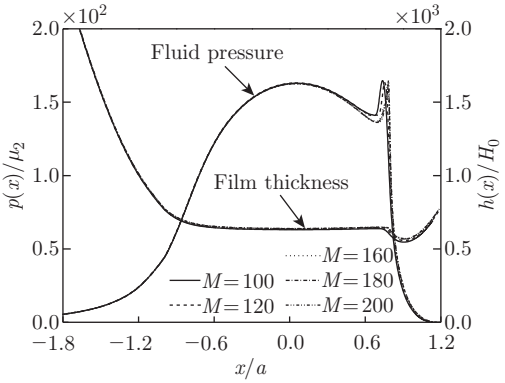

Fig. 6 Effect of discrete node number M on the fluid pressure $p(x)$ and film thickness $h(x)$ with $R = 100\,\mu\text{m}$, $V_0 = 0.5\,\text{mm/s}$, $l = 0.6\,\mu\text{m}$, $H = 1.0\,\mu\text{m}$, $\mu_1/\mu_2 = 1.2$, $S = 0$, and $P = 350\,\text{N/m}$

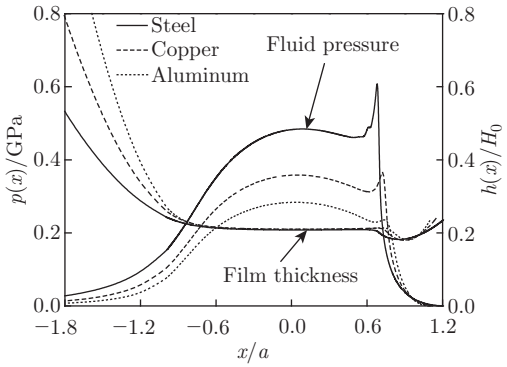

Fig. 7 Effect of different materials on fluid pressure $p(x)$ and film thickness $h(x)$

4.2 EHL contact analysis

The effect of size parameter on $p(x)$, $h(x)$, and $\sigma_{xx1}(x, H)$ is analyzed in Fig. 8. In-plane stress $\sigma_{xx1}(x, H)$ in Fig. 8(b) is taken at the surface of the coating, i.e., $y = H$. As expected, $h(x)$, $p(x)$, and $\sigma_{xx1}(x, H)$ are significantly affected by l. Moreover, Fig. 8 also plots the classical result for $l = 0$. It is clearly observed that the fluid pressure at the whole EHL contact region is enlarged distinctly due to the appearance of the size effect. Therefore, neglect of the size effect could result in the underestimation of the results at micro-/nano-scale EHL. Pressure spike emerging close to the contact outlet enlarges with the increase of l. Size effect reduces $h(x)$ at the inlet, but enlarges it at center and outlet. $h(x)$ gets small at the inlet and center with l increasing from $0.3\,\mu\text{m}$ to $2.0\,\mu\text{m}$, while it is slightly affected at the outlet. In particular, the outlet with minimum film thickness is prone to severe wear. For the classical elasticity ($l = 0$), the in-plane stress $\sigma_{xx1}(x, H)$ reaches its maximum near the contact center, and it is compressive at all locations. For couple-stress elasticity, $\sigma_{xx1}(x, H)$ is still compressive at the whole lubricant region for a small l. But, with the increase of l, compressive stress gradually transforms to tensile stress at the center, and maximum tensile stress appears at the outlet. Because different asymptotic values f_{11} are obtained in couple-stress elastic contact $(-1/(\mu_1(6 - 4\nu_1)))$[14,23] and classical elastic contact $((1 - 2\nu_1)/(2\mu_1))$[42]. These two values have opposite signs. This explains the change of $\sigma_{xx1}(x, H)$ from compressive ones to tensile ones in couple-stress elastic contact with l increasing.

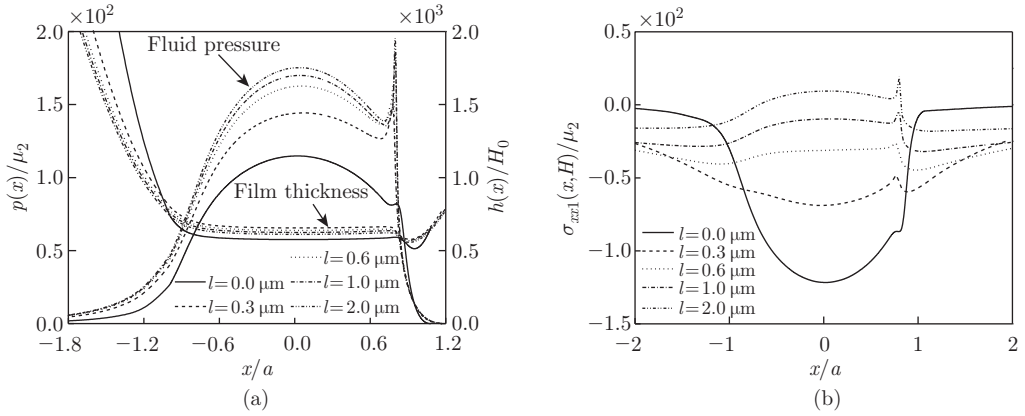

Fig. 8 Effect of size parameter l on (a) fluid pressure $p(x)$, film thickness $h(x)$, and (b) in-plane stress $\sigma_{xx1}(x, H)$ with $R = 100\,\mu\text{m}$, $V_0 = 0.5\,\text{mm/s}$, $H = 1.0\,\mu\text{m}$, $\mu_1/\mu_2 = 1.2$, $S = 0$, and $P = 350\,\text{N/m}$

Figure 9 shows the effect of the stiffness ratio μ_1/μ_2 on $h(x)$ and $p(x)$. When μ_1/μ_2 changes from 1/1.4 to 1.4, i.e., the coating becomes stiffer and stiffer, $p(x)$ becomes greater at the whole EHL contact region. Particularly, with μ_1/μ_2 increasing, the pressure spike increases distinctly at the outlet and moves forward slightly. The effect of μ_1/μ_2 is pronounced on fluid pressure, but slight on film thickness. The increase of μ_1/μ_2 reduces $h(x)$ at the inlet, and slightly enlarges it at the center and outlet. These results suggest that distributions of film thickness and fluid pressure can be changed by modifying stiffness ratio. Hence, coatings can be effectively employed to improve contact damage of material surfaces in EHL contact.

The effect of coating thickness H on $h(x)$ and $p(x)$ is plotted in Fig. 10. The presence of the coating yields a remarkable increase in fluid pressure, while reduces film thickness at inlet of EHL contact region. However, the coating has little effect on $h(x)$ at center and outlet. With the increase of H from 0 μm to 5 μm, the fluid pressure shows an increasing trend.

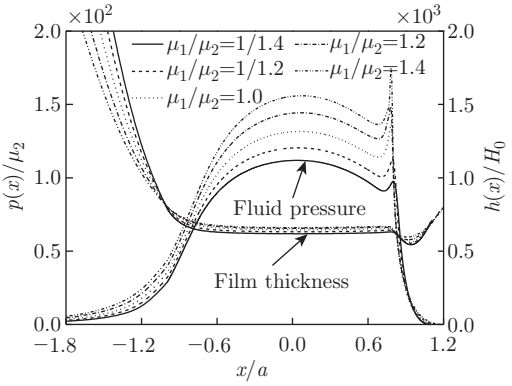

Fig. 9 Effect of stiffness ratio μ_1/μ_2 on fluid pressure $p(x)$ and film thickness $h(x)$ with $R = 100\,\mu\text{m}$, $V_0 = 0.5\,\text{mm/s}$, $H = 1.0\,\mu\text{m}$, $l = 0.3\,\mu\text{m}$, $S = 0$, and $P = 350\,\text{N/m}$

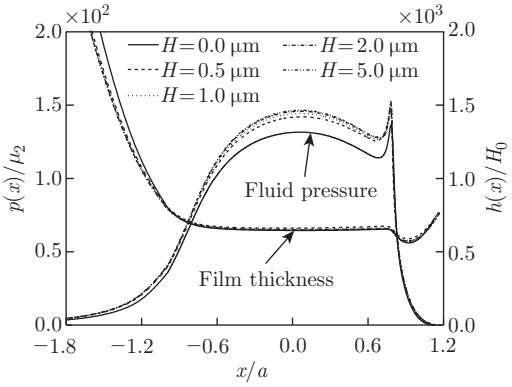

Fig. 10 Effect of coating thickness H on fluid pressure $p(x)$ and film thickness $h(x)$ with $R = 100\,\mu\text{m}$, $V_0 = 0.5\,\text{mm/s}$, $\mu_1/\mu_2 = 1.2$, $l = 0.3\,\mu\text{m}$, $S = 0$, and $P = 350\,\text{N/m}$

Figure 11 illustrates the effect of entraining velocity V_0 on $p(x)$, $h(x)$, and $\sigma_{xx1}(x,H)$. As V_0 increases, pressure spike tends to move forward and becomes large, and $h(x)$ increases at the EHL contact region. $\sigma_{xx1}(x,H)$ is compressive at the whole lubricant region, and maximum compressive stress appears at the contact center. V_0 has little effect on in-plane stress $\sigma_{xx1}(x,H)$.

Figure 12 gives the effect of slide/roll ratio S on $p(x)$, $h(x)$ and $\sigma_{xx1}(x,H)$. The slide-roll ratio S is very essential in this study. $S=0$ implies pure rolling condition, i.e., $V_1=V_2$, while $S=2$ for pure sliding condition, i.e., $V_1=0$. Moreover, results of Newtonian fluid are also presented. It is found that results of Newtonian and non-Newtonian fluid models are identical for $S=0$. S has a great effect on pressure spike at the outlet, whereas it has little effect on film thickness and in-plane stress. An increase of S yields a remarkable decrease of pressure spike. Interestingly, the similar influencing trend of S can also be found in the study of the classical EHL contact[48–49].

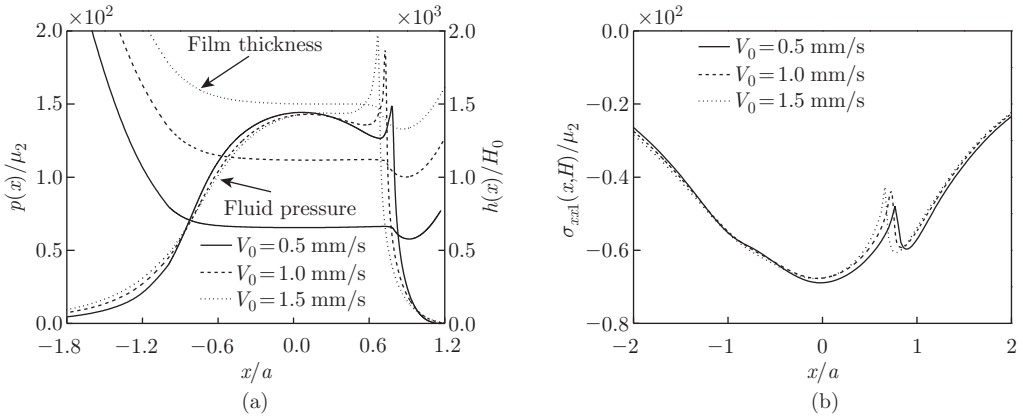

Fig. 11 Effect of entrainment velocity V_0 on (a) fluid pressure $p(x)$, film thickness $h(x)$, and (b) in-plane stress $\sigma_{xx1}(x,H)$ with $R=100\,\mu$m, $H=1.0\,\mu$m, $\mu_1/\mu_2=1.2$, $l=0.3\,\mu$m, $S=0$, and $P=350\,$N/m

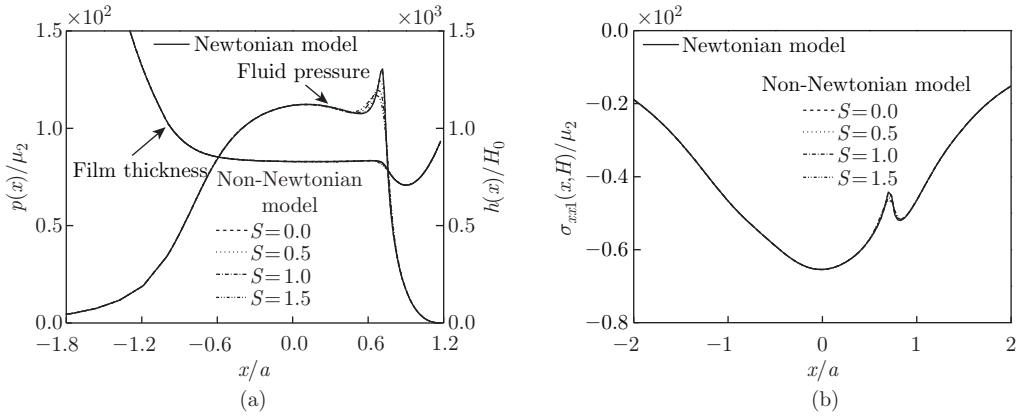

Fig. 12 Effect of slide/roll ratio S on (a) fluid pressure $p(x)$, film thickness $h(x)$, and (b) in-plane stress $\sigma_{xx1}(x,H)$ with $H=1.0\,\mu$m, $V_0=0.5\,$mm/s, $\mu_1/\mu_2=1.2$, $l=0.3\,\mu$m, $R=150\,\mu$m, and $P=350\,$N/m

Figure 13 illustrates the variation of $h(x)$ and $p(x)$ with the resultant normal load P. As P increases, the fluid pressure increases at center, but pressure spike moves backward and decreases. $h(x)$ decreases with P increasing at center and outlet.

Figure 14 discusses the effect of punch radius R on $h(x)$ and $p(x)$. With R increasing, $h(x)$ increases but $p(x)$ decreases at the EHL contact region. The increase of R results in the forward movement of pressure spike.

Figure 15 plots the effect of slide/roll ratio S on shear stress $\tau_1(x)$ at the coating surface $y = H$ for non-Newtonian fluid. When S changes from 0 to 2, the shear stress $\tau_1(x)$ becomes greater at the whole EHL contact region, and its maximum value appears near the outlet.

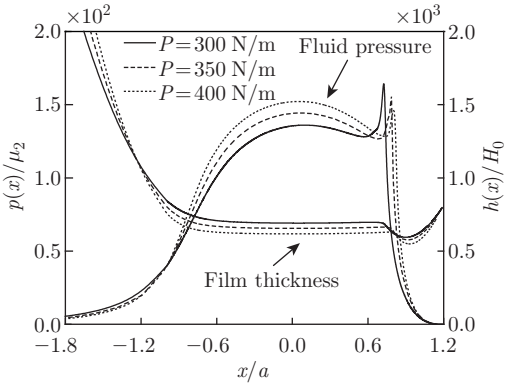

Fig. 13 Effect of resultant normal load P on fluid pressure $p(x)$ and film thickness $h(x)$ with $R = 100\,\mu\text{m}$, $V_0 = 0.5\,\text{mm/s}$, $\mu_1/\mu_2 = 1.2$, $l = 0.3\,\mu\text{m}$, $S = 0$, and $H = 1.0\,\mu\text{m}$

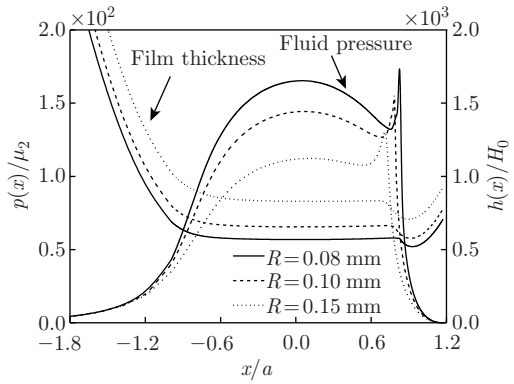

Fig. 14 Effect of punch radius R on fluid pressure $p(x)$ and film thickness $h(x)$ with $H = 1.0\,\mu\text{m}$, $V_0 = 0.5\,\text{mm/s}$, $\mu_1/\mu_2 = 1.2$, $l = 0.3\,\mu\text{m}$, $S = 0$, and $P = 350\,\text{N/m}$

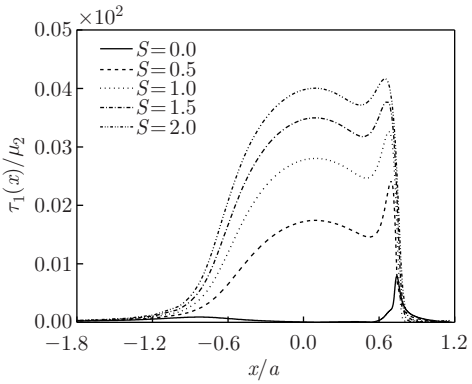

Fig. 15 Effect of slide/roll ratio S on shear stress $\tau_1(x)$ with $H = 1.0\,\mu\text{m}$, $V_0 = 0.5\,\text{mm/s}$, $\mu_1/\mu_2 = 1.2$, $l = 0.3\,\mu\text{m}$, $R = 150\,\mu\text{m}$, and $P = 350\,\text{N/m}$

Figure 16 illustrates the effect of slide/roll ratio S on frictional coefficient T/P for Newtonian and non-Newtonian fluid. T is the resultant tangential load on the coating surface ($y = H$), i.e., $T = \int_{x_{\text{in}}}^{x_{\text{out}}} \tau_1(x)\mathrm{d}x$. With the increase of S, the frictional coefficient increases linearly for Newtonian fluid, while it increases nonlinearly for the non-Newtonian fluid. This results from the shear thinning effect of non-Newtonian fluid.

Note that the numerical results in Figs. 8–10 and 14 are obtained for a constant normal load P. Therefore, the integral of $p(x)$ over the contact region should be a constant (i.e., $\int_{x_{\text{in}}}^{x_{\text{out}}} p(x)\mathrm{d}x = P$). However, an apparent violation is observed in these figures due to the use of normalized contact region ($x_{\text{in}}/a \leqslant x/a \leqslant x_{\text{out}}/a$), other than the actual contact region ($x_{\text{in}} \leqslant x \leqslant x_{\text{out}}$). As we know, a changes for different size parameter l, stiffness ratio μ_1/μ_2, coating thickness H or punch radius R when P is fixed. We choose the normalized transverse coordinate as x/a in order to compare the pressure spike and its location.

In the above analysis, the size parameters of the coating and the half-plane are considered as the same value. However, the size parameters of the coating and the half-plane may be different. Therefore, we need to consider the effect of the size parameter ratio on the fluid pressure and film thickness. Figure 17 shows the effect of the size parameter ratio l_1/l_2 on $p(x)$ and $h(x)$. When l_1/l_2 changes from 0.5 to 2.0, the fluid pressure $p(x)$ becomes greater at the whole EHL contact region. $h(x)$ gets small at the inlet with l_1/l_2 increasing, while it is slightly affected at the center and outlet.

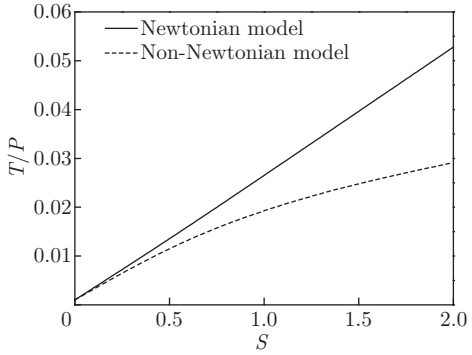

Fig. 16 Variation of frictional coefficient versus slide/roll ratio S with $H = 1.0\,\mu\text{m}$, $V_0 = 0.5\,\text{mm/s}$, $\mu_1/\mu_2 = 1.2$, $l = 0.3\,\mu\text{m}$, $R = 150\,\mu\text{m}$, and $P = 350\,\text{N/m}$

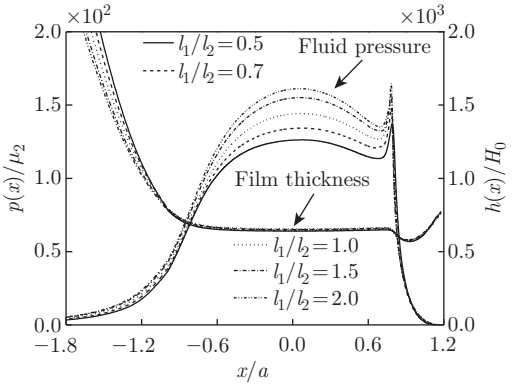

Fig. 17 Effect of size parameter ratio l_1/l_2 on fluid pressure $p(x)$ and film thickness $h(x)$ with $H = 1.0\,\mu\text{m}$, $V_0 = 0.5\,\text{mm/s}$, $\mu_1/\mu_2 = 1.2$, $l = 0.3\,\mu\text{m}$, $R = 150\,\mu\text{m}$, $S = 0$, and $P = 350\,\text{N/m}$

It should be pointed out that the present paper focuses on the EHL contact of the cylindrical punch based on the couple stress theory. Our results in Fig. 8 show that the fluid pressure increases as the size parameter increases from $0\,\mu\text{m}$ to $0.2\,\mu\text{m}$. However, Song et al.[23] investigated the dry contact problem for both cylindrical punch and flat punch based on the couple stress theory. Their results for the cylindrical punch have the similar trend with that of the present paper, but the trend for the flat punch is different. For the flat punch, the pressure distribution first departs from and then approaches the classic result as the size parameter increases from $0\,\mu\text{m}$ to $0.2\,\mu\text{m}$. Similar phenomenon was also observed by Zisis et al.[14] for flat punch and cylindrical punch.

5 Conclusions

We analyze size-dependent EHL line contact by employing the couple-stress elasticity theory. A deformable homogeneous coated half-plane and the rigid cylindrical punch are separated by a non-Newtonian lubricant. An iterative method is conducted to calculate film thickness, in-plane stress, and fluid pressure. The following results can be obtained.

(I) When the size effect is considered, the fluid pressure is enlarged at the whole EHL contact

region, and the film thickness is enlarged at center and outlet, but reduced at the inlet. With the increase of the size parameter, in-plane stress gradually transforms from the compressive to the tensile at the center. The film thickness is slightly affected at the outlet, but decreases at inlet and center as the size parameter increases.

(II) As the stiffness ratio increases, fluid pressure becomes greater at the whole EHL contact region and pressure spike moves forward slightly, and film thickness increases slightly at center and outlet.

(III) The presence of the coating enlarges the fluid pressure at the whole EHL contact region but decreases the film thickness at inlet, and has little influence on film thickness at outlet and center. With the increase of coating thickness, the fluid pressure shows an increasing trend.

(IV) An increase in the slide/roll ratio results in a significant decrease of pressure spike at the outlet, whereas it has little influence on the film thickness.

References

[1] CHEN, P., CHEN, S., and PENG, J. Interface behavior of a thin-film bonded to a graded layer coated elastic half-plane. *International Journal of Mechanical Sciences*, **115-116**, 489–500 (2016)

[2] BJORLING, M., LARSSON, R., and MARKLUND, P. The effect of DLC coating thickness on elstohydrodynamic friction. *Tribology Letters*, **55**, 353–362 (2014)

[3] GUO, Y. B., LU, X. Q., LI, W. Y., and HE, T. Interfacial stress and failure analysis for piston ring coatings under dry running condition. *Tribology Transactions*, **356**, 1027–1034 (2013)

[4] CHU, L. M., CHEN, C. Y., TEE, C. K., CHEN, Q. D., and LI, W. L. Elastohydrodynamic lubrication analysis for transversely isotropic coating layer. *Journal of Tribology*, **136**, 031502 (2014)

[5] CHEN, Z., GOLTSBERG, R., and ETSION, I. A universal model for a frictionless elastic-plastic coated spherical normal contact with moderate to large coating thicknesses. *Tribology International*, **114**, 485–493 (2017)

[6] COMEZ, I. and ERDOL, R. Frictional contact problem of a rigid stamp and an elastic layer bonded to a homogeneous substrate. *Archive of Applied Mechanics*, **83**, 15–24 (2013)

[7] YAN, J. and MI, C. W. On the receding contact between an inhomogeneously coated elastic layer and a homogeneous half-plane. *Mechanics of Materials*, **112**, 18–27 (2017)

[8] STAN, G. and ADAMS, G. G. Adhesive contact between a rigid spherical indenter and an elastic multi-layer coated substrate. *International Journal of Solids and Structures*, **87**, 1–10 (2016)

[9] ZHANG, X. L., LAUWERENS, W., STALS, L., HE, J. W., and CELIS, J. P. Fretting wear rate of sulphur deficient MoSx coatings based on dissipated energy. *Journal of Materials Research*, **16**, 3567–3574 (2001)

[10] HABCHI, W. Influence of thermo-mechanical properties of coatings on friction in elastohydrodynamic lubricated contacts. *Tribology International*, **90**, 113–122 (2015)

[11] HE, T., WANG, Z. J., and WU, J. Q. Effect of imperfect coating on the elastohydrodynamic lubrication: dislocation-like and force-like coating-substrate interfaces. *Tribology International*, **143**, 106098 (2020)

[12] HU, J. J., SUN, W. M., JIANG, Z. H., ZHANG, W., LU, J. W., HUO, W. T., ZHANG, Y. S., and ZHANG, P. X. Indentation size effect on hardness in the body-centered cubic coarse grained and nanocrystalline tantalum. *Materials Science and Engineering*: *A*, **686**, 19–25 (2017)

[13] MINDLIN, R. D. and TIERSTEN, H. F. Effects of couple-stresses in linear elasticity. *Archive for Rational Mechanics and Analysis*, **11**, 415–448 (1962)

[14] ZISIS, T., GOURGIOTIS, P. A., BAXEVANAKIS, K. P., and GEORGIADIS, H. G. Some basic contact problems in couple stress elasticity. *International Journal of Solids and Structures*, **51**, 2084–2095 (2014)

[15] NEFF, P., MÜNCH, I., GHIBA, I. D., and MADEO, A. On some fundamental misunderstandings in the indeterminate couple stress model. *International Journal of Solids and Structures*, **81**, 233–243 (2016)

[16] SHAAT, M. Physical and mathematical representations of couple stress effects on micro/nanosolids. *International Journal of Applied Mechanics*, **7**, 1550012 (2015)

[17] GOURGIOTIS, P. A. and ZISIS, T. Two-dimensional indentation of microstructured solids characterized by couple-stress elasticity. *The Journal of Strain Analysis for Engineering Design*, **51**, 318–331 (2015)

[18] ZISIS, T., GOURGIOTIS, F., and CORSO, D. A. Contact problem in couple stress thermoelasticity: the indentation by a hot flat punch. *International Journal of Solids and Structures*, **63**, 226–239 (2015)

[19] SONG, H. X., KE, L. L., and WANG, Y. S. Sliding frictional contact analysis of an elastic solid with couple stresses. *International Journal of Mechanical Sciences*, **133**, 804–816 (2017)

[20] WANG, Y. X., SHEN, H. M., ZHANG, X., ZHANG, B., LIU, J., and LI, X. Y. Semi-analytical study of microscopic two-dimensional partial slip contact problem within the framework of couple stress elasticity: cylindrical indenter. *International Journal of Solids and Structures*, **138**, 76–86 (2018)

[21] BHATTACHARYYA, A. S. and MISHRA, S. K. Micro/nano-mechanical behaviour of magnetron sputtered Si-C-N coatings through nanoindentation and scratch tests. *Journal of Micromechanics and Microengineering*, **21**, 015011 (2011)

[22] KARURIYA, A. N. and BHANDAKKAR, T. K. Plane strain indentation on finite thickness bonded layer in couple stress elasticity. *International Journal of Solids and Structures*, **108**, 275–288 (2017)

[23] SONG, H. X., KE, L. L., WANG, Y. S., YANG, J., and JIANG, H. Two-dimensional frictionless contact of a coated half-plane based on couple stress theory. *International Journal of Applied Mechanics*, **10**, 1850049 (2018)

[24] FIROUZ-ABADI, R. D., MOHAMMAD-KHANI, H., and RAHMANIAN, M. Vibration and stability analysis of DWCNT-based spinning nanobearings. *International Journal of Structural Stability and Dynamics*, **17**, 1750102 (2017)

[25] ELSHARKAWY, A. A., HOLMES, M. J. A., EVANS, H. P., and SNIDLE, R. W. Micro-elastohydrodynamic lubrication of coated cylinders using coupled differential deflection method. *Proceedings of the Institution of Mechanical Engineers, Part J: Journal of Engineering Tribology*, **220**, 29–41 (2006)

[26] XIAO, Z. L. and SHI, X. Tribological and thermal properties of a crowned gear pair with high-speed and heavy-load in thermal micro-elastohydrodynamic lubrication. *Proceedings of the Institution of Mechanical Engineers, Part J: Journal of Engineering Tribology*, **234**, 541–553 (2019)

[27] SHIRVANI, K. A., MOSLEH, M., and SMITH, S. T. Nanopolishing by colloidal nanodiamond in elastohydrodynamic lubrication. *Journal of Nanoparticle Research*, **18**, 248 (2016)

[28] WOLOSZYNSKI, T., TOUCHE, T., PODSIADLO, P., STACHOWIAK, G. W., CAYER-BARRIOZ, J., and MAZUYER, D. Effects of nanoscale ripple texture on friction and film thickness in EHL contacts. *Tribology Letters*, **67**, 16 (2019)

[29] CHECO, H. M., DUREISSEIX, D., FILLOT, N., and RAISIN, J. A homogenized micro-elastohydrodynamic lubrication model: accounting for non-negligible microscopic quantities. *Tribology International*, **135**, 344–354 (2019)

[30] MIHAILIDIS, A., AGOURIDAS, K., and PANAGIOTIDIS, K. Non-Newtonian starved thermal-elastohydrodynamic lubrication of finite line contacts. *Tribology Transactions*, **56**, 88–100 (2013)

[31] TANNER, R. I. *Engineering Rheology*, Clarendon, Oxford (1988)

[32] REE, T. and EYRING, H. Theory of non-Newtonian flow. I, solid plastic system. *Journal of Applied Physics*, **26**, 793–809 (1955)

[33] JOHNSON, K. L. and TEVAARWERK, J. L. Shear behaviour of elastohydrodynamic oil films. *Proceedings of the Royal Society of London A*, **356**, 215–236 (1977)

[34] BAIR, S. and WINER, W. O. A rheological model for EHL contacts based on primary laboratory data. *Journal of Lubrication Technology*, **101**, 258–265 (1979)

[35] KIM, K. H. and SADEGHI, F. Non-Newtonian elastohydrodynamic lubrication of point contacts. *Journal of Tribology*, **113**, 703–711 (1991)

[36] CUI, J., YANG, P., JIN, Z. M., and DOWSON, D. Transient elastohydrodynamic analysis of elliptical contacts. Part 3: non-Newtonian lubricant solution under isothermal and thermal conditions. *Proceedings of the Institution of Mechanical Engineers*, *Part J*: *Journal of Engineering Tribology*, **221**, 63–73 (2007)

[37] GWINNER, J. Frictional unilateral contact for hemitropic solids in micropolar elasticity and boundary element approximation. *Applications of Mathematics in Engineering and Economics*: *AIP Conference Proceedings*, **1789**, 040030 (2016)

[38] YANG, P. and WEN, S. A generalized Reynolds equation for non-Newtonian thermal elastohydrodynamic lubrication. *Journal of Tribology*, **112**, 631–636 (1990)

[39] DOWSON, D. A generalized Reynolds equation for fluid film lubrication. *International Journal of Mechanical Sciences*, **4**, 159–170 (1962)

[40] YANG, P. R. and WEN, S. Z. A forward iterative numerical method for steady-state elastohydrodynamically lubricated line contacts. *Tribology International*, **23**, 17–22 (1990)

[41] CASTLE, P. and DOWSON, D. A theoretical analysis of the starved elastohydrodynamic lubrication problem for cylinders in line contact. *Elastohydrodynamic Lubrication* 1972 *Symposium*, University of Leeds, Leeds (1972)

[42] JOHNSON, K. L. *Contact Mechanics*, Combridge University Press, Cambridge (1985)

[43] GRADSHTEYN, I. S. and RYZHIK, I. M. *Table of Integrals*, *Series*, *and Products*, Academic, New York (2000)

[44] ERDOGAN, F. and GUPTA, G. D. On the numerical solution of singular integral equations. *Quarterly of Applied Mathematics*, **29**, 525–534 (1972)

[45] DOWSON, D. and HIGGINSON, G. R. A numerical solution to the elastohydrodynamic problem. *Journal Mechanical Engineering Science*, **1**, 6–15 (1959)

[46] SU, J., SONG, H. X., and KE, L. L. Elastohydrodynamic lubrication line contact in couple-stress elasticity. *Mathematics and Mechanics of Solids*, **26**, 1053–1073 (2021)

[47] LI, K. Y. and HOOKE, C. J. Non-Newtonian effects in rough EHL contacts. *Transient Processes in Tribology*, **43**, 167–177 (2004)

[48] LEE, R. T. and HAMROCK, B. J. A circular non-Newtonian fluid model: part I—used in elastohydrodynamic lubrication. *Journal of Tribology*, **112**, 486–496 (1990)

[49] ELSHARKAWY, A. A. and HAMROCK, B. J. EHL of coated surfaces: part II—non-Newtonian results. *Journal of Tribology*, **116**, 786–793 (1994)